AN INVESTIGATION OF FUNDAMENTAL FLOW STRUCTURES IN GROUND EFFECT WITH APPLICATION TO THE DEVELOPMENT OF BROWNOUT CONDITIONS IN HOVER

K. Bourne[1], K.R. Reddy[1], C. Kumar[1], and A. Ooi[2]

[1]Defence Science and Technology Organisation
506 Lorimer St, Fishermans Bend, Victoria 3207
Australia

[2]Melbourne University
Parkville, Melbourne, Victoria 3100
Australia

ABSTRACT

The flow structures underlying the formation of toroid-like dust clouds during brownout are not well understood. This study sought to confirm the presence of persistent structures, referred to here as global recirculation, which would correlate with anecdotal evidence indicating such structures were stable rather than transient. Both stereo and planar Particle Image Velocimetry (PIV) was used to assess the flow beneath a sub-scale rotor model operating in ground effect. Results showed that a global recirculation flow structure could be generated at 200 and 300 RPM, and although persistent, there was evidence of the structure meandering over time.

1. INTRODUCTION

The rotor wake flow characteristics associated with helicopter operations in level and vertical flight are quite well understood, and the theory describing such regimes is reasonably mature; however, this does not extend to phenomena associated with aerodynamic interference effects. The interaction between the main rotor wake and external objects, such as buildings, ship structures and ground planes, as well as impingement of the rotor downwash on airframe components, result in highly complex flow conditions. In particular, the disturbance of sand and dust particles by the rotor wake during low altitude, low speed flight and hover in ground effect (IGE) can lead to significant operational difficulty. Such conditions are commonly referred to as brownout.

Brownout is a complex aerodynamic environment characterised by the entrainment of small ground particles by the rotor. When brownout conditions are fully developed, cockpit visibility is wholly obscured by the dust particles entrained by the helicopter rotor wake. In such instances aircrew can rapidly lose situational awareness, significantly increasing the probability of a mishap during non-automated landings*. The 2010 study by Couch and Lindell [1] assessed rotorcraft safety and survivability within the US Department of Defense, focusing on mishaps that occurred during Operation Enduring Freedom and Operation Iraqi Freedom. Brownout was a primary causal factor and accounted for 24% of rotary wing non-hostile combat losses.

Brownout presents the greatest hazard to operations during landing manoeuvres, when the pilot's awareness of aircraft attitude and motion are most critical. It should be noted that the risks associated with takeoff manoeuvres in brownout conditions are not considered as significant when compared to the corresponding risk of landing manoeuvres. The extent to which visual cues are lost, particularly the loss of ground and horizon references, dictates the severity of the brownout conditions from a pilot perspective. If sight of the ground can be maintained during the final phases of the descent, anecdotal evidence indicates the risk of mishap are significantly reduced [2]. Of particular interest to this study is the region of air close to the fuselage, which ultimately dictates the quality of the useable cue environment (UCE). Brownout dust cloud characteristics are highly variable, however the development of a very large cloud does not automatically equate to a degradation in UCE. In some instances the region of clear air close to the fuselage is maintained throughout landing, despite development of a large cloud beyond the periphery of the rotor disk.

Fundamentally, brownout is a phenomenon comprising the flow structure of a helicopter rotor wake as well as the motion of particles. The rotor wake flow structure is dictated by the helicopter flight characteristics and its proximity to the ground, whereas particle motion depends on the size, shape and mass of the particles at the ground surface. As such, the range of factors capable of influencing the development of brownout conditions is extensive, ranging from aircraft-specific details such as the rotor characteristics, to the environmental conditions

* The advancement of control system "upper modes", which in some cases enable full automation of vertical landing manoeuvres, has proven beneficial to operations in brownout-prone areas. Such modes are generally features of current-generation aircraft and represent technology that is not easily retrofitted to older fleets. In addition, automated landings are not always feasible within every operational context, and so do not yet represent a full solution to safe operations in brownout conditions.

on the day. Put simply, it is not yet possible to generalise or accurately predict the characteristics of the brownout clouds using simulation or modelling techniques, owing to the complexity of the problem.

Research into the brownout phenomena represents a large body of work, ranging from fundamental investigation of the underlying fluid mechanics of the problem [3,4,5,6] to the development and prototyping of devices and procedures aimed to improve the safety of operations [7,8,9]. As has been noted by a number of authors [10,11], accurate simulation of brownout conditions is a challenging task, and model validation is notoriously difficult owing to a very small set of suitable flight-trial data [12,13]. In response to such issues, several sub-scale experiments have looked to improve the understanding of the intricacies of rotor wake flow fields IGE [14,15].

2. BACKGROUND

This study was originally intended as an investigation into the possible development of aerodynamic devices designed to mitigate brownout conditions during landing manoeuvres in hover†. In low speed forward flight IGE, a ground vortex is formed ahead of the rotor as shown in Figure 1. The strength of the ground vortex is maximal around 15-20 kt forward speed, before becoming weak and breaking down at approximately 30 kt. The ground vortex plays a critical role in the entrainment of particles ahead of the rotor during non-vertical landing and low altitude manoeuvres, and is accepted as the primary cause of brownout flow structures ahead of the aircraft.

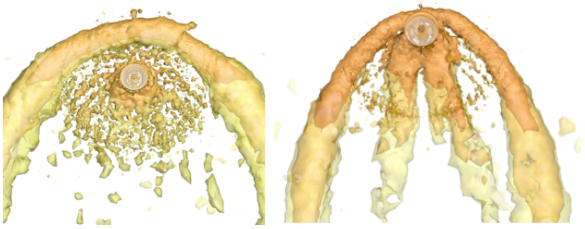

Figure 1: *Ground vortex at (a) 10 kt and (b) 20 kt (image taken from [16])*

For cases of true vertical descent and hover IGE, where there is no aircraft drift, forward speed or ambient wind, the ground vortex does not develop. Instead, the blade tip vortices dominate the flow structure, creating the distinctive flow pattern seen in Figure 2 (left). Viewed from above, the dust cloud formed in nil wind conditions looks like a toroid, as seen in Figure 2 (right), with the strength of the vorticity dictated by aircraft characteristics and the descent rate. The fluid mechanics underlying this flow structure are not well understood, specifically with regard to the persistent nature of the toroid structure and the associated region of clear air near the aircraft fuselage.

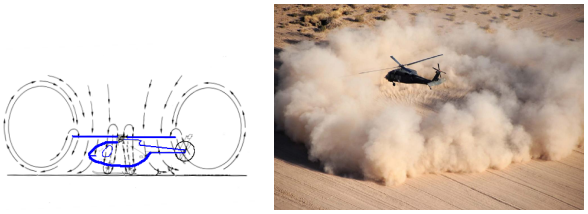

Figure 2: *Schematic of helicopter IGE‡ (left) and brownout conditions developing (right)*

It is hypothesised that for the case of true hover IGE, it is possible for a "global recirculation" flow structure to exist, which perpetuates the toroidal flow structure, as shown in Figure 2 (left) above. The rotor wake behaviour most likely to cause such structures would be a persistent up-flow, whereby some percentage of the radially-expanding wake turns back towards the rotor disk rather than following the ground plane. This theory was proposed after anecdotal evidence implied the toroid structure was stable, and not transient.

An initial investigation assessed the potential of both passive and active deflectors to influence the region of flow near to the fuselage, which extended to particular focus on the performance of a basic active deflector [17]. Inherent to this approach were the following suppositions relating to the flow field present during brownout conditions:

1. Maintaining a region of clear air close to the fuselage for the duration of a landing manoeuvre will increase the safety of operations.
2. The airflow inboard of the blade tip vortices is a comparatively weak component of the rotor wake downwash, without distinct structure.
3. The presence of a global recirculation zone is primarily responsible for the dimensions of the region of clear air near to the cockpit.
4. Influencing the global recirculation zone could influence the geometry and persistence of the region of clear air.

† As distinct from landing manoeuvres involving forward speed or headwinds.

‡ Image a modified version of that presented by R. Prouty, *Helicopter Aerodynamics – The Rotor Wake*

Although the overarching motivation was to investigate aerodynamic methods by which the risks posed by brownout during vertical landings may be ameliorated, a thorough understanding of the fundamental flow field remained the prime concern. An assessment of the effect of dust particles on the rotor wake was considered beyond the scope of the study. As such, it was assumed that the motion of the dust particles would follow the motion of the air without altering the flow structure, although it is acknowledged that such an assumption will not always be valid.

Results of the deflector testing did show a region of weak recirculation inboard of the slipstream boundary created by the blade tip vortices, which could be influenced by the active deflector; however there was no evidence of a global recirculation trend. Given the intent of the deflectors was to influence the geometry of the toroid structure, the current investigation focused on whether global recirculation could be reproduced sub-scale.

3. EXPERIMENTAL SETUP AND SYSTEM DESCRIPTION

The experiments were conducted in the Defence Science and Technology Organisation (DSTO) Low Speed Wind Tunnel (LSWT) using both two-dimensional, two-component (2D-2C) planar and two-dimensional, three-component (2D-3C) stereo Particle Image Velocimetry (PIV). The region of interest was illuminated using a New Wave Solo PIV 200XT Nd:YAG dual-pulse laser, with a laser sheet thickness of 2 mm. Images were acquired using TSI PowerView^{TM} Plus CCD camera(s), fitted with a 200 mm Micro Nikkor f/4 lens set to F#8. The CCD camera has a pixel resolution of 4008 x 2672, a pixel size of 9 μm x 9 μm and a frame rate of 2.07 Hz in frame straddling mode. Figure 3 shows the equipment configuration for both the stereo and planar measurements. The PIV seed particles were Di-2-EthylHexyl-Sebacate (commonly referred to as DEHS) droplets generated using a Laskin nozzle. Data acquisition and processing was completed using the TSI INSIGHT^{TM} 4G software.

Testing was undertaken with two, small-scale two-bladed rotors, details of which are provided in Table 1. Both blades used a NACA0012 aerofoil section and had a radius (R) of 70 mm, without twist or camber. Each was manufactured as a single piece, as shown in Figure 4, with a fixed angle of attack (α). A Hall-Effect sensor was mounted to the rotor shaft and used to trigger the PIV data acquisition at a blade azimuth angle of 90°, which ensured the blade was clear of the recorded image. The maximum acquisition rate of the equipment (2 Hz) was below the nominal operational speeds of the rotor (3 – 17 Hz), and as such the results could be phase-averaged but not time-averaged.

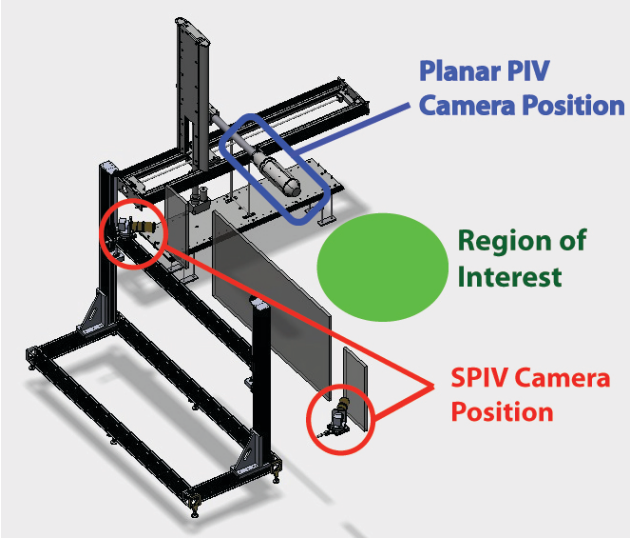

Figure 3: *PIV camera configurations*

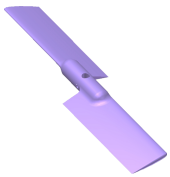

Figure 4: *Rotor blade*

Table 1: *Rotor blade specifications*

Blade Designation	***Chord (mm)***	***α***
B1	15	12°
B2	20	15°

4. PIV PROCESSING

4.1 Stereo PIV

Experimental setup for the 2D-3C Stereo PIV (SPIV) yielded a reproduction ratio of 7.9 and a spatial resolution of 70.86 μm/pixel. Based on the requirement that the maximum particle displacement be less than 25% of the initial interrogation window (IW) size of 64 × 64 pixels, the time interval between laser pulses (Δt) was determined individually for each test case.

The data was processed through a two-pass recursive algorithm using 50% grid spacing overlap. The first pass IW was 64 × 64 pixels, and the resultant particle image displacement distance then applied to the second pass with an IW size of 32 × 32 pixels. Offsetting the IW by the particle image

displacement distance increases the signal-to-noise ratio, as lost pairs due to in-plane motion are reduced. Spurious vectors were removed using a global velocity range filter, a mean filter using a neighbourhood size of 3 x 3 pixels and a displacement tolerance of 2 pixels for each test case. Vectors identified as invalid were replaced with interpolated points using bi-linear interpolation.

Data convergence was assessed using running averages of the turbulence intensity and velocity components. All results stabilised within the first 500 samples and did not show accumulative bias error, indicating sufficient convergence in the statistical parameters could be established from the number of vector fields recorded for each test case. To reduce measurement uncertainty, between 1000 – 3000 image pairs were acquired for each test case.

4.2 Planar PIV

Experimental setup for the 2D-2C planar PIV yielded a reproduction ratio of 8.0 and a spatial resolution of 136 μm/pixel. As for SPIV, the time interval between laser pulses (Δt) was determined individually for each test case and the data was processed through a two-pass recursive algorithm using 50% grid spacing overlap. The 2D data set was processed with a first pass IW of 32 × 32 pixels, reducing to 16 × 16 pixels second pass. As previously, the vector fields were validated via a global and local velocity range filter.

5. RESULTS

5.1 Stereo PIV

SPIV was undertaken to assess the flow field generated by blades B1 and B2, which were installed at a one rotor diameter (1D) height above the ground plane. The nominal rotation speed was varied between 200 – 1000 RPM (3.33 – 16.67 Hz). Presented in Figures 5-7 are the mean velocity magnitude contour plots for several test cases, along with the corresponding vector field. The vertical axes on each graph, representing rotor height above the ground plane (z), has been non-dimensionalised by the rotor diameter (D), whereas the horizontal axis, displaying distance from the rotor shaft centreline (x), has been non-dimensionalised by the rotor radius (R). In all cases the location of the rotor Tip Path Plane (TPP) has been included for reference.

Figure 5 shows the results for B1 and B2 at 200 RPM. Evident in both mean flow fields is a recirculating region of flow, the structure of which is consistent with the hypothesis of global recirculation. The relative magnitude of the up-flow is quite weak compared to the velocity of the wake at the ground plane; however, its geometry is consistent with what would be expected for a flow structure underlying a global toroidal flow. The effect of increase in thrust is seen in the differences between the B1 and B2 results, with the increase in downwash velocity acting to move the centre of the recirculation zone further from the rotor centreline.

Figure 6 shows the results for B1 and B2 at 300 RPM. Unlike the flow fields observed at 200 RPM, there was no evidence of a global recirculation region at 300 RPM. This result also extended to the flow fields developed at 500 and 1000 RPM, shown in Figure 7, where no evidence of large-scale flow recirculation was observed. It was proposed that the absence of such structures could be due to limitations of the Field Of View (FOV). Specifically, that the rotor downwash deflected by the ground plane had not yet slowed sufficiently so as to generate recirculation within the FOV.

5.2 Planar PIV

To increase the FOV and further assess the flow structures observed at 200 RPM, the PIV setup was changed to a planar configuration. Of particular interest was the repeatability and persistence of the flow conditions, and the effect of changes in thrust and rotor height above the ground plane on the global recirculation structures.

Figure 8 presents the mean velocity magnitude results for blades B1 and B2 at 200 RPM and a distance of 1D from the ground plane. In both cases, a region of global recirculation is evident. Unlike the SPIV results, the centre of the recirculation is closer to the rotor shaft for the B2 test case. Given that the data sets presented in Figures 5 and 8 are averaged flow fields, the change in radial location of the up-flow may be indicative of flow structure meandering.

Although the flow condition is repeatable, there is movement of the structure over time[§]. This hypothesis is confirmed by examination of the instantaneous vector fields, an example of which is included in Appendix A. It can be seen that the location and geometry of the up-flow region, and the associated global recirculation, meanders in the radial direction. Rather than a progressive change, the flow structures oscillate radially both inward and

[§] Limitations associated with mechanical components of the rotor rig meant that there was minor fluctuation in the rotor RPM up to +/-5%, despite the use of a feedback controller. As a source of experimental error it was deemed acceptable, but is a factor likely to contribute to flow structure instabilities.

outward. Although it is not possible to determine whether these fluctuations are a result of the inherent instability of the structure, or whether they are driven by small variations in the rotor RPM; it is proposed that the helical vortex wake may be behaving like a system of vortex rings, where wake radial geometry varies with time.

Shown in Figure 9 are the mean velocity magnitude results at 200 RPM and a distance of 0.75D from the ground plane. The global recirculation is still evident for the B1 test case, and there is an up-flow trend for B2; however the mean flow field does not conclusively capture the centre of recirculation. Examination of the instantaneous flow field results confirms the presence of up-flow and recirculation, but the centre of the recirculation meanders in both the vertical and radial directions. When compared to the 200 RPM results at 1D, refer Figure 9, there is similarity in both the magnitude of the up-flow and global recirculation structures.

Test cases at 300 and 500 RPM were also assessed to confirm the results of the SPIV experiments. Figure 10 presents the mean velocity magnitude at 300 RPM for the blades B1 and B2 at a distance of 1D from the ground plane. Unlike the SPIV mean flow fields generated under the same test conditions; the planar PIV results show some evidence of a global recirculation flow structure. The lower thrust conditions generated by B1 show a more pronounced region of recirculation than the comparatively weak up-flow generated by B2. Decreasing the distance between the rotor and the ground plane to 0.75D changed the geometry of the recirculation region, as shown in Figure 11.

In both cases the strength of the recirculation region was decreased, and the centre of rotation of the global recirculation increased in height above the ground plane. It is not possible to draw firm conclusions for the B2 test case, owing to the fact the flow structure has moved beyond the FOV of the camera at 0.75D, but there is still some evidence of large-scale recirculation. These results were not seen in the SPIV experiments due to the fact that the up-flow initiated beyond the FOV of the camera. Increasing the size of the region of interest for the 2D-2C analysis enabled the larger flow structures to be captured.

The mean flow fields generated by B1 and B2 at 500 RPM did not show evidence of global recirculation flow structures.

6. DISCUSSION

The differences in the flow structure generated by blades B1 and B2 are relatively consistent between test cases. Blade B1 produces a more pronounced up flow and recirculation pattern, despite the proportionate decrease in flow velocity. The more detailed flow structure seen in the 200 RPM SPIV results of Figure 5 show that the core of the global recirculation region is closer to the rotor shaft and lower to the ground in the B1 flow field than it is for the flow generated by B2, however the difference in the core location is not large.

At 300 RPM, refer Figure 6, the strength of the up-flow and global recirculation regions is reduced compared to the 200 RPM flow fields. The up-flow region generated by B1 is more pronounced than for B2, and the B2 recirculatory flow feature is also markedly weaker, so much so that it is not readily discernable in the mean velocity magnitude contour plot. The geometry of the B1 structure is similar at both RPM, however the B2 structure appears to flatten out with the 100 RPM increase.

The effect of decreasing the rotor height above the ground did not have as significant an effect as was expected. In each test case the increased proximity to the ground increased the velocity of the flow at the ground plane as expected, but it was not possible to identify a clear trend relating to the effect on the subsequent geometry of the up-flow or global recirculation structures.

The mean flow fields for all B1 test cases consistently exhibit up-flow and global recirculation structures. The higher thrust conditions produced by the B2 blade profile show higher variability in results, with the up-flow and recirculation present during the 200 RPM, 1D test case no longer clearly evident in the mean flow field results for 300 RPM at 0.75D. Comparing the mean velocity magnitude results between test cases, it can be seen that changes in rotor blade profile and RPM have different effects on the geometry of the flow structure; despite the fact each variable ostensibly alters the thrust being generated.

7. CONCLUDING REMARKS

Of the data analysed to date, there is good evidence that a global recirculation flow structure was generated beneath the IGE rotor at 200 and 300 RPM. Comparison of the mean flow field results and instantaneous vector fields indicates that the structure meanders radially, and that the centre of the recirculation zone also fluctuates in height.

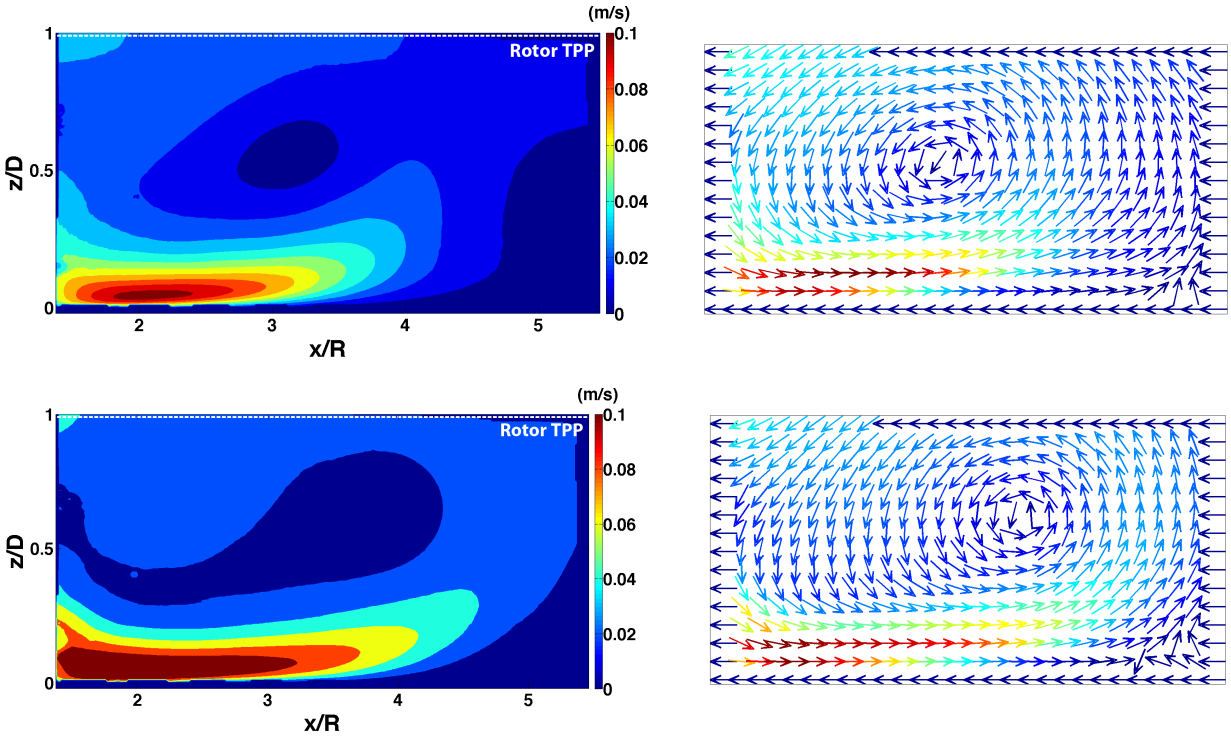

Figure 5: *SPIV mean velocity magnitude contour plots (left) and corresponding vector flow fields (right) generated by B1 (top) and B2 (bottom) at 200 RPM, z/D=1.*

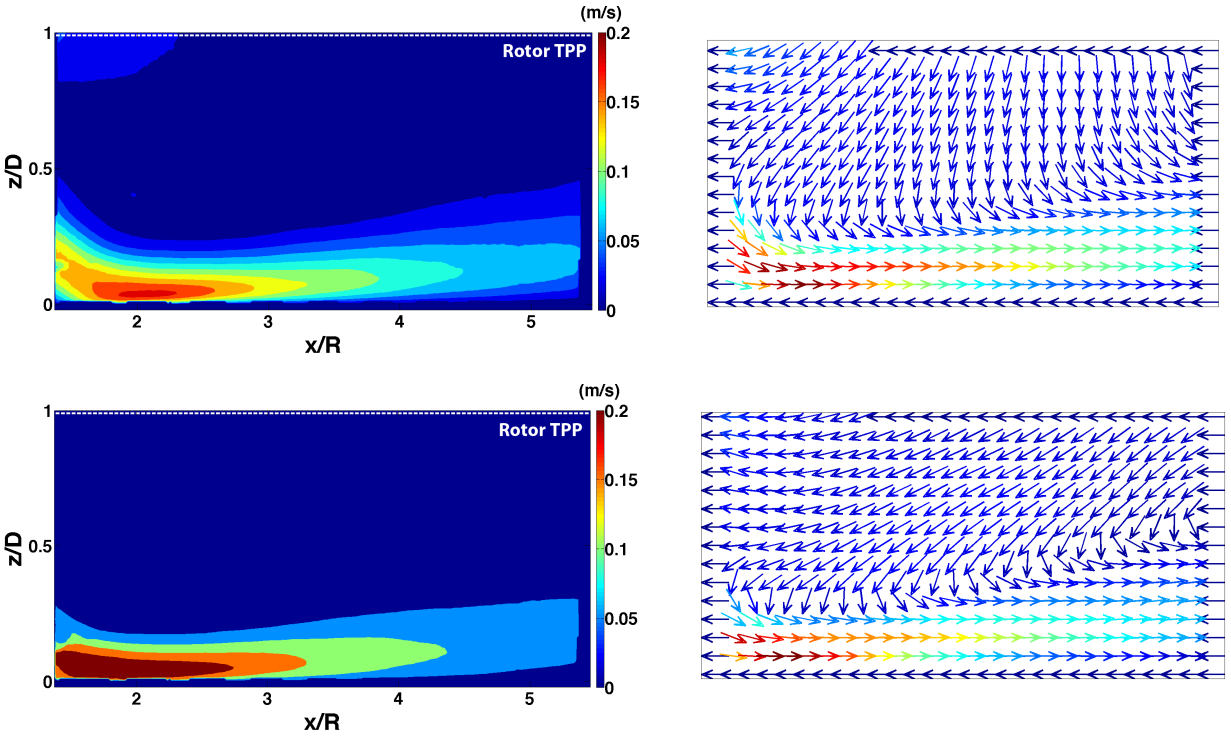

Figure 6: *SPIV mean velocity magnitude contour plots (left) and corresponding vector flow fields (right) generated by B1 (top) and B2 (bottom) at 300 RPM, z/D=1.*

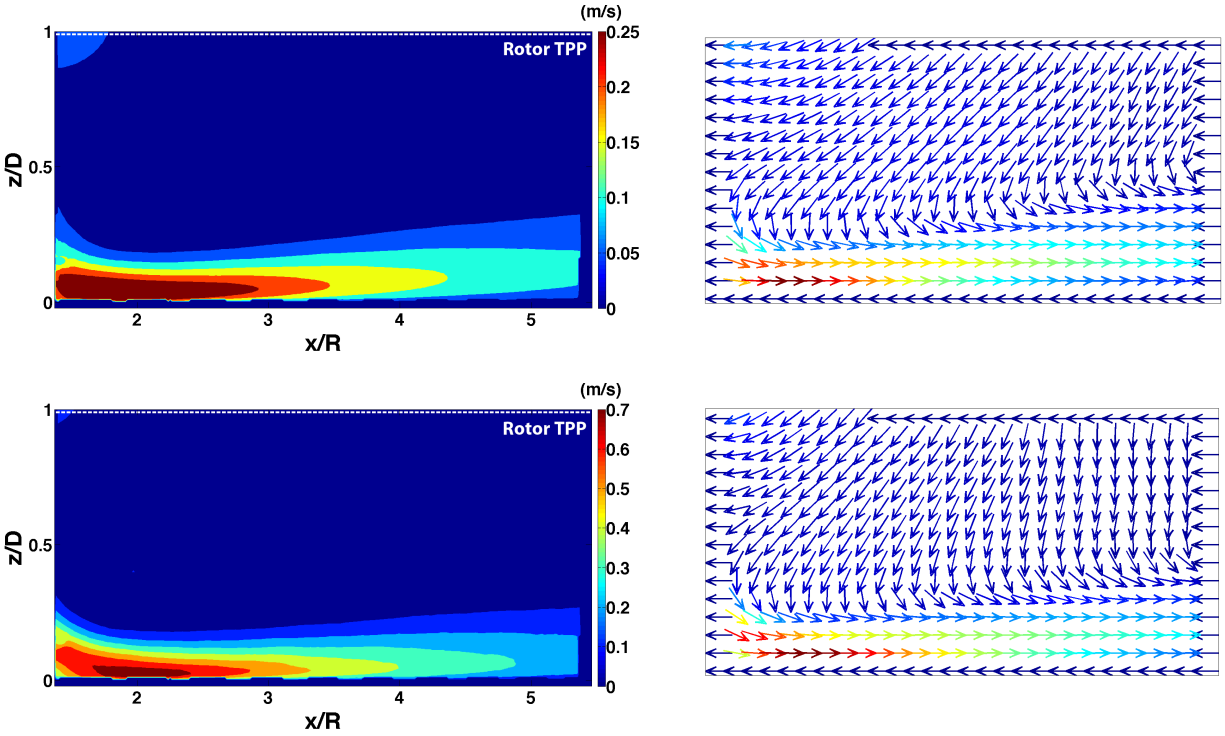

Figure 7: *SPIV mean velocity magnitude contour plots (left) and corresponding vector flow fields (right) generated by B1 at (top) 500 RPM and (bottom) 1000 RPM, z/D=1.*

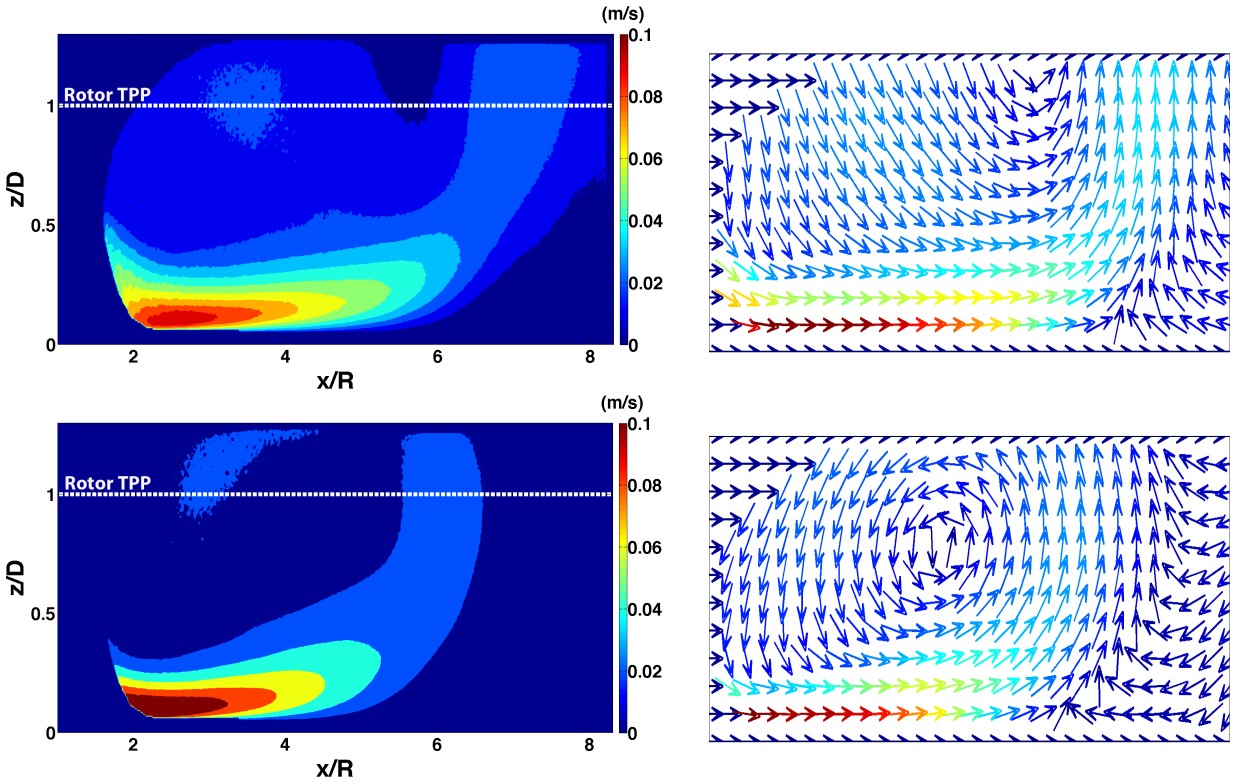

Figure 8: *Planar PIV mean velocity magnitude contour plots (left) and corresponding vector flow fields (right), generated by B1 (top) and B2 (bottom) at 200 RPM, z/D=1.*

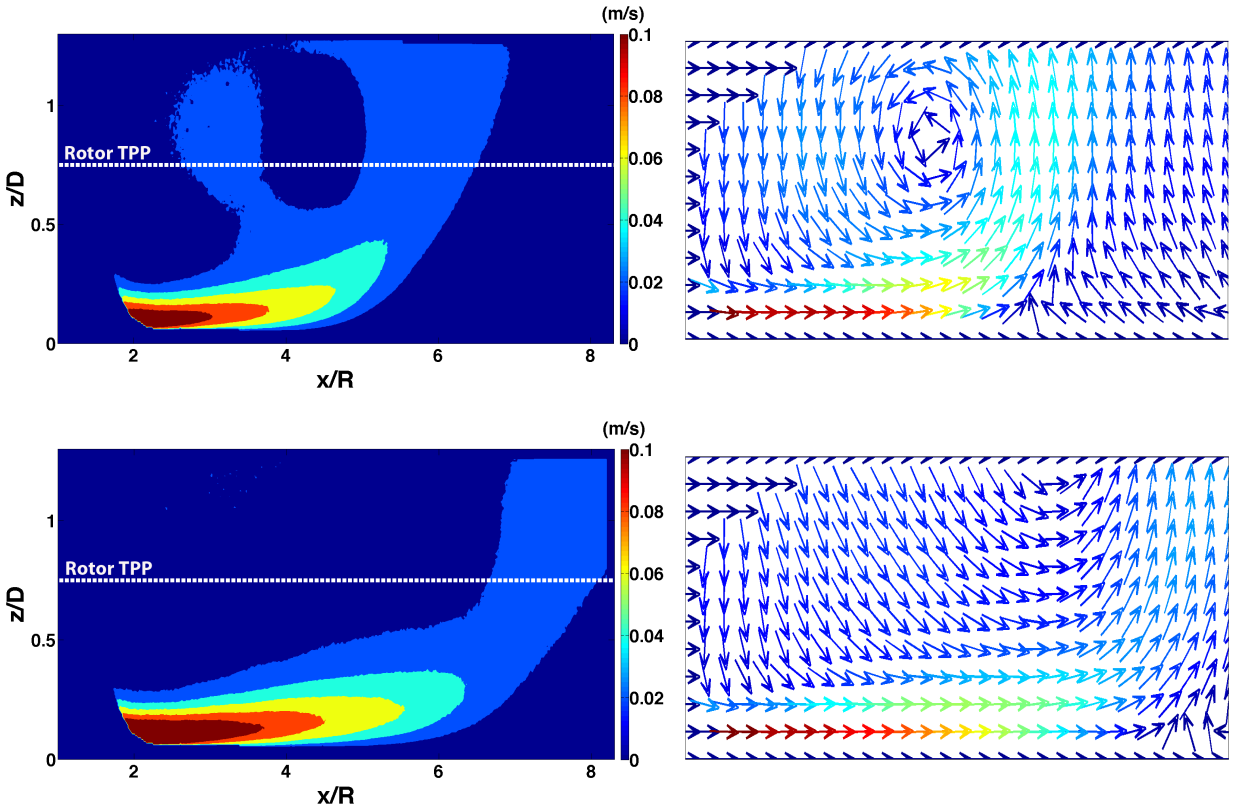

Figure 9: *Planar PIV mean velocity magnitude contour plots (left) and corresponding vector flow fields (right) generated by B1 (top) and B2 (bottom) at 200 RPM, z/D=0.75.*

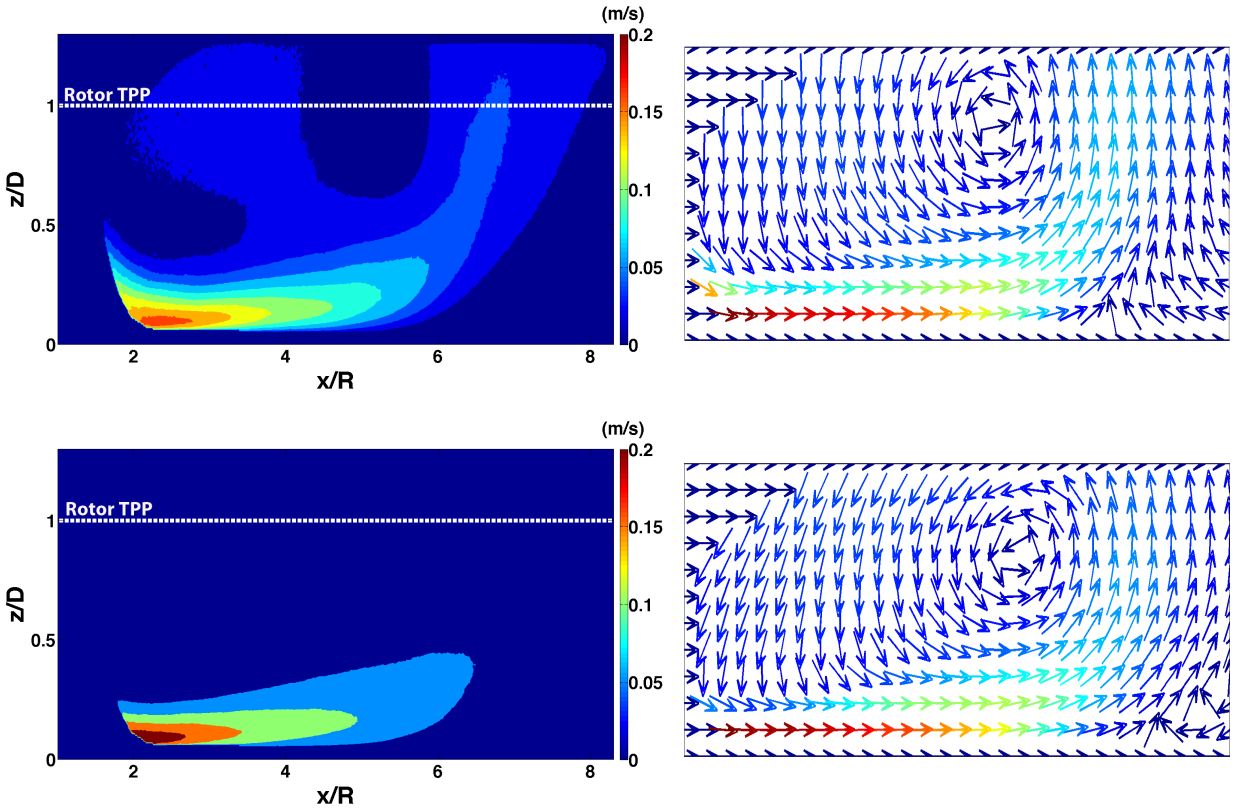

Figure 10: *Planar PIV mean velocity magnitude contour plots (left) and corresponding vector flow fields (right) generated by B1 (top) and B2 (bottom) at 300 RPM, z/D=1.*

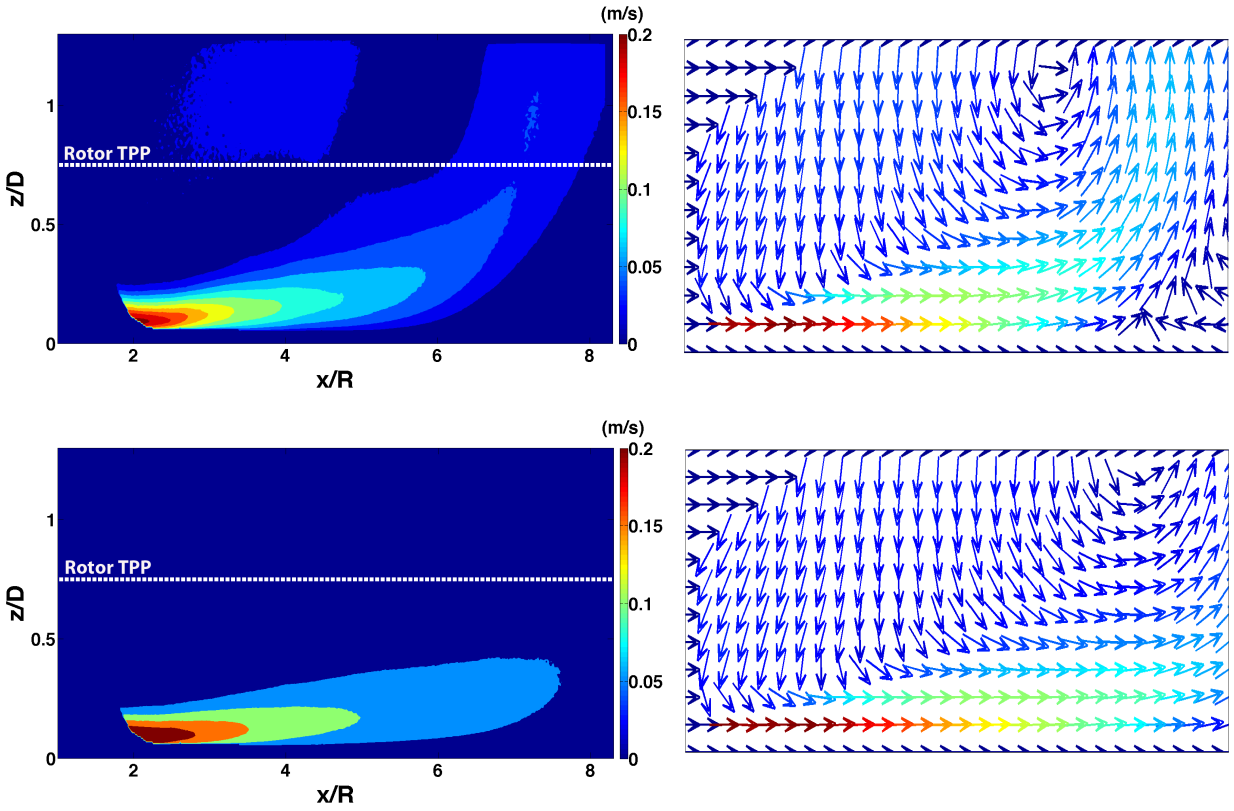

Figure 11: *Planar PIV mean velocity magnitude contour plots (left) and corresponding vector flow fields (right) generated by B1 (top) and B2 (bottom) at 300 RPM, z/D=0.75.*

8. ACKNOWLEDGEMENTS

The authors wish to gratefully acknowledge the assistance of Peter Manovski and Matteo Giacobello for their advice and guidance during testing, and for their technical support thanks to Paul Jacquemin, John Clayton, John Xiberras, Brett Lemke and Paul Vella. Thanks also to Soon-Kong Lee.

9. REFERENCES

[1] Couch, M.and D. Lindell. *Study on Rotorcraft Safety and Survivabilty.* American Helicopter Society 66th Annual Forum, Pheonix, AZ, May 11-13, 2010.

[2] Bourne, K., S. Manso, R. Widjaja et al. *MRH 90 Reduced Visibility Operations Trial: Dust Cloud Characterisation.* DSTO-TR-2984, Defence Science and Technology Organisation, Melbourne, Australia, June 2014.

[3] Lee, T.E., J.G. Leishman and M. Ramasamy. *Fluid Dynamics of Interacting Blade Tip Vortices With a Ground Plane.* American Helicopter Society 64th Annual Forum, Montreal, Canada, April 29 – May 1, 2008.

[4] Nathan, N. and R.B. Green. *Measurements of a rotor flow in ground effect and visualization of the brown-out phenomenon.* American Helicopter Society 64th Annual Forum, Montreal, Canada, April 29 – 1 May, 2008.

[5] Rauleder, J. and J.G. Leishman. *Flow Environment and Organized Turbulence Structures at the Ground Below a Rotor.* American Helicopter Society 68th Annual Forum, Fort Worth, TX, May 1-3, 2012.

[6] Jasion, G. and J. Shrimpton. *Prediction of Brownout Inception Beneath a Full-Sclae Helicopter Downwash.* Journal of the American Helicopter Society, **57** (4), 2012, 1-13.

[7] Harrington, W., S. Braddom, J. Savage, Z. Szoboszlay, R.A. McKinley and H.N. Burns. *3D-LZ Brownout Landing Solution.* American Helicopter Society 66th Annual Forum, Pheonix, AZ, May 11-13, 2010.

[8] NATO Research and Technical Organisation, *Rotary-Wing Brownout Mitigation: Technologies and Training*. Technical Report TR-HFM-162, January 2012.

[9] Tritschler, J., R. Celi and J.G. Leishman. *A Methodology for Rotorcraft Brownout Mitigation Through Flight Path Optimization.* American Helicopter Society 68th Annual Forum, Fort Worth, TX, May 1-3, 2012.

[10] Thomas, S., V.K. Lakshminarayan, T.S. Kalra and J.D. Baeder. *Eulerian-Lagrangian Analysis of Cloud Evolution using CFD Coupled with a Sediment Tracking Algorithm.* American Helicopter Society 67th Annual Forum, Virginia Beach, VA, May 3-5, 2011.

[11] D'Andrea, A. *Numerical Analysis of Unsteady Vortical Flows Generated by a Rotorcraft Operating on Ground: A First Assessment of Helicopter Brownout*. American Helicopter Society 65th Annual Forum, Grapevine, TX, May 27-29, 2009.

[12] Cowherd, C. *Sandblaster 2 Support of See-Through Technologies for Particulate Brownout.* Final Technical Report, Midwest Research Institute, Kansas City, October 2007.

[13] Wong, O.D. and P.E. Tanner, *Photogrammetric Measurements of an EH-60L Brownout Cloud.* American Helicopter Society 66th Annual Forum, Phoenix, AZ, May 11-13, 2010.

[14] Sydney, A., A. Baharani and J.G. Leishman. *Understanding Brownout using Near-Wall Dual-Phase Flow Measurements.* American Helicopter Society 67th Annual Forum, Virginia Beach, VA, May 3-5, 2011.

[15] Sydney, A. and J.G. Leishman, *Measurements of Rotor/Airframe Interactions in Ground Effect Over a Sediment Bed.* American Helicopter Society 69th Annual Forum, Phoenix, AZ, May 21-23, 2013.

[16] Reddy, K.R., R. Widjaja, K. Bourne and S. Wahono. *Flow Simulation of Helicopter Operations in Close Proximity to the Ground.* 11th Engineering Mathematics and Applications Conference, December 1-4, 2013.

[17] Bourne, K., P. Manovski, K.R. Reddy and A. Ooi. *Experimental Evaluation of the Effect of Flow Deflectors on Helicopter Rotor Wake Vortices.* 18th Australasian Fluid Mechanics Conference, Launceston, Australia, December 3-7 2012.

Appendix A: Instantaneous Vector Fields

Shown in the figure below are instantaneous vector fields selected at random from each data set. They are placed in temporal order[**], but are not sequential.

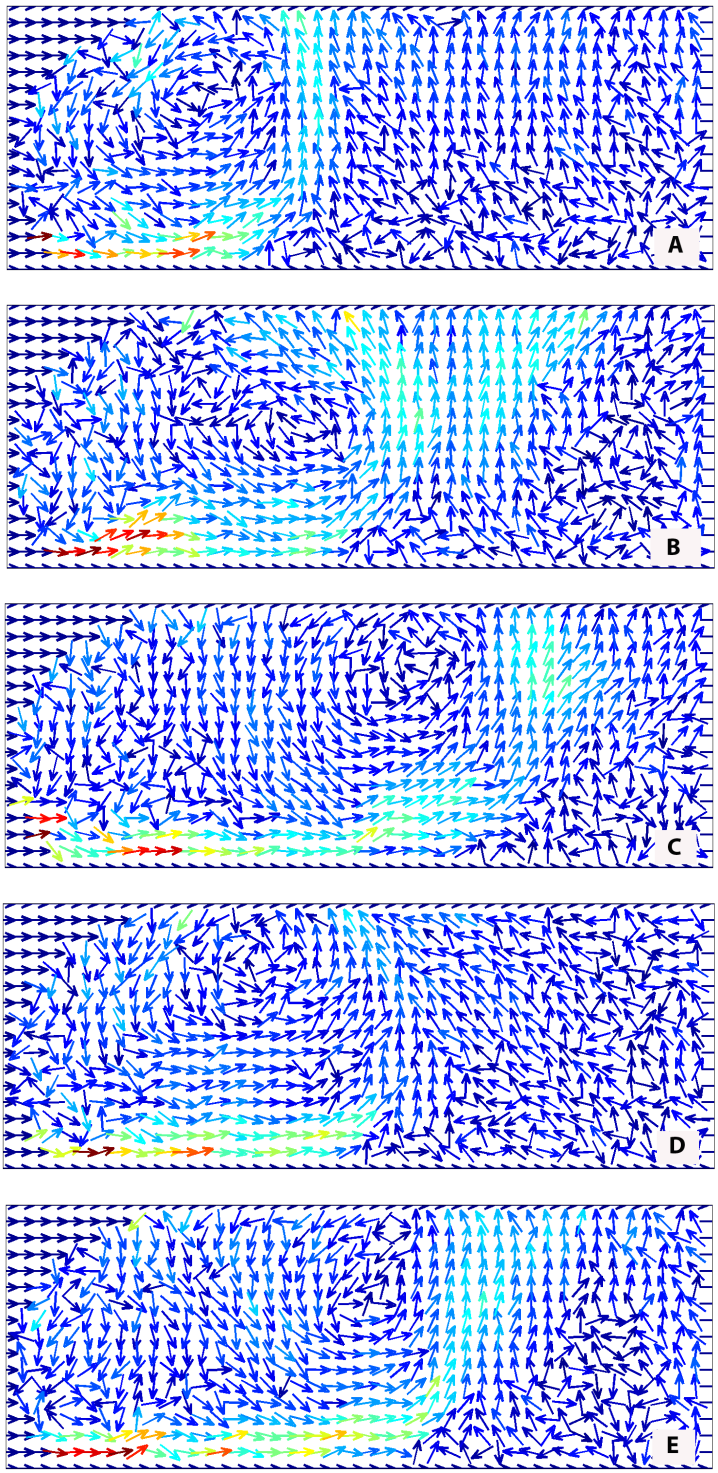

Figure A1: *Instantaneous vector fields captured with blade B1 at 0.75D*

[**] Image (A) was captured prior to image (B), which in turn was captured prior to image (C) etc.